npj | vaccines

Article

Published in partnership with the Sealy Institute for Vaccine Sciences

https://doi.org/10.1038/s41541-024-00979-w

DNA vaccines against GPRC5D synergize with PD-1 blockade to treat multiple myeloma

Check for updates

Praveen Neeli[1] ✉, Perry Ayn Mayson A. Maza[1], Dafei Chai[1], Dan Zhao[1], Xen Ping Hoi[2], Keith Syson Chan[2], Ken H. Young[3] & Yong Li[1] ✉

Multiple myeloma (MM), a hematological malignancy of the bone marrow, remains largely incurable. The orphan G protein-coupled receptor, GPRC5D, which is uniquely expressed in plasma cells and highly expressed in MM, is a compelling candidate for immunotherapy. In this study, we investigated the efficacy of a combination of DNA vaccine encoding mouse GPRC5D and PD-1 blockade in preventing and treating MM using the 5TGM1 murine model of MM. The mouse vaccine alone was effective in preventing myeloma growth but required PD-1 antibodies to inhibit established MM tumors. We next evaluated the prophylactic and therapeutic efficacy of a nanoplasmid vector encoding human GPRC5D in several murine syngeneic tumor models. Similar results for tumor inhibition were observed, as human GPRC5D-specific T cells and antibodies were induced by DNA vaccines. Taken together, these findings underscore the potential of GPRC5D-targeted DNA vaccines as versatile platforms for the treatment and prevention of MM.

Multiple myeloma (MM), the second most prevalent hematological malignancy, is characterized by the accumulation of malignant plasma cells in the bone marrow[1,2]. Almost all MM cases are preceded by monoclonal gammopathy of undetermined significance (MGUS)[3]. A diagnosis of MGUS may reduce a person's life expectancy by more than 4 years[3]. MGUS affects approximately 3.5 million people in the US, which is 3.2% of the total population aged over 50 years[4]. Smoldering MM (SMM) is an asymptomatic clonal plasma cell disorder between MGUS and MM. SMM is distinguished from MGUS primarily for clinical reasons because the risk of progression to malignancy is 10% per year for SMM vs. 1% per year for MGUS[3,5,6].

The treatment of MM has been transformed with the advent of antibody-based therapies, including anti-CD38 antibodies, bispecific antibodies, and chimeric antigen receptor (CAR) T-cell therapies[7–10]. CAR-T-cell therapies targeting the B-cell maturation antigen (BCMA) have shown considerable promise[11]. Two CAR T therapies targeting BCMA, namely ciltacabtagene autoleucel (Carvykti) and idecabtagene vicleucel (Abecma), have been approved by the United States Food and Drug Administration (FDA) for the treatment of MM. Despite the widespread expression of BCMA in most malignant plasma cells, the pattern of its expression is heterogeneous, which is responsible for varied treatment responses[12]. Additionally, the surface expression of BCMA may fluctuate over time because of gamma secretase-mediated shedding of its extracellular domain[13]. In addition, antigen escape, such as downregulation of BCMA, has been documented in patients with MM who experienced relapse following BCMA-targeted CAR T-cell therapy, similar to the relapses observed after CD19- and CD22-targeted CAR T-cell therapies for B-cell malignancies[14–17]. Therefore, exploring immunotherapies targeting alternative antigens may help counteract antigen escape and provide effective treatment options for patients who relapse after BCMA-targeted CAR T-cell treatment.

G protein-coupled receptors (GPCRs) are the largest and most diverse group of membrane receptors in eukaryotes. Humans have nearly 1000 different GPCRs that play major roles in the cAMP and phosphatidylinositol signaling pathways in response to various external signals[18]. Approximately 35% (700) of the FDA-approved drugs target more than 135 GPCRs[19,20]. GPCRs are classified into six classes (A–F). Class C GPCRs initiate several metabolic steps that modulate cellular activity. Orphan GPCR class C group 5 member D (GPRC5D) is expressed in two anatomical locations, namely the hair follicle (an immune-privileged site) and the bone marrow of patients with MM[21], as well as in MGUS and SMM[22,23]. The GPRC5D mRNA is overexpressed two to four times in MM plasma cells compared with that in normal plasma cells, and intermediate GPRC5D expression is observed in MGUS and SMM[22,23]. Therefore, GPRC5D is an emerging novel immunotherapeutic and preventive target for MM[21,22,24,25].

[1]Department of Medicine, Baylor College of Medicine, Houston, TX, 77030, USA. [2]Department of Urology, Neal Cancer Center, Houston Methodist Research Institute, Houston, TX, USA. [3]Department of Pathology, Division of Hematopathology, Duke University Medical Center, Durham, NC, USA. ✉e-mail: neelipraveen@gmail.com; yong.li@bcm.edu

DNA vaccines offer a promising approach to cancer prevention and treatment in which protein antigens are delivered to elicit cellular and humoral immunity. Despite their lower cost and better stability than those of mRNA vaccines, DNA vaccines have not yet been widely adopted in clinical practice. The development of DNA vaccine therapeutics for cancer faces significant challenges, including nonspecific formulations, thermal instability, toxicity, and ineffectiveness. However, recent advancements in delivery systems, adjuvants, prime-boost strategies, immune checkpoint blockade, improved vectors, and immunostimulatory signals have greatly enhanced the clinical efficacy of DNA vaccines in cancer treatment. In this study, we aimed to develop DNA vaccines against MM using plasmids expressing GPRC5D. We first evaluated a mouse GPRC5D DNA vaccine in the 5TGM1 murine myeloma model. Next, we assessed the efficacy of the human GPRC5D DNA vaccine using the MC38 murine model. These vaccines exhibited strong antitumor effects in a prophylactic setting. In a therapeutic setting, the vaccines exhibited moderate antitumor activities and could inhibit MM when used in conjunction with a monoclonal antibody against PD1 (PD1 Ab). This study provides a proof-of-concept for targeting GPRC5D using DNA vaccines for MM prevention and intervention.

Results

The mouse GPRC5D vaccine inhibits tumor growth in a 5TGM1 murine model of MM

We first assessed the efficacy of the mouse GPRC5D vaccine in a 5TGM1 murine model of MM, that closely mimics human MM. The 5TGM1 MM cells arising spontaneously in aging C57BL/KaLwRij mice were propagated via serial passages in syngeneic mice prior to the establishment of a cell line[26,27]. We confirmed endogenous GPRC5D expression on the surface of 5TGM1 cells using western blotting and flow cytometry analyses (Fig. 1A, B). Next, we generated a DNA construct expressing mouse GPRC5D using the gWIZ vector (gWIZ-mGPRC5D). We first examined the cancer prevention activity by administering the DNA vaccine before tumor cell inoculation (Fig. 1C). We immunized the host C57BL/KaLwRij mice following a prime-boost schedule at 2-week intervals, delivering 20 μg of the gWIZ-mGPRC5D plasmid or a control plasmid intramuscularly (IM) followed by electroporation (EP) using the ICHOR Trigrid device. Eight days after booster immunization, each mouse received a subcutaneous (SC) injection of 3×10^5 5TGM1 cells in the right flank. Mice administered the mGPRC5D vaccine developed significantly smaller tumors than did the control mice ($p < 0.001$; Fig. 1D, E). By day 33, all animals in the mGPRC5D group were alive, whereas all control mice reached the humane endpoint. Next, we evaluated the humoral response using ELISA to measure the levels of mGPRC5D-specific antibody in the serum collected 5 days after the boost. A marked increase in serum IgG levels was noted in the mGPRC5D group compared with that in the control group (Fig. 1F). Furthermore, we explored the potential mechanisms underlying the antitumor effect of the mGPRC5D vaccine by analyzing immune cells in the spleen and tumors using flow cytometry. The percentage of various immune cell populations, including $CD3^+$, $CD3^+CD4^+$, and $CD3^+CD8^+$ T cells, dendritic cells (DCs, $CD45^+CD11c^+$), macrophages (Mϕ, $CD45^+CD11b^+F4/80^+$), and natural killer (NK, $CD45^+CD3^-NK1.1^+$) cells significantly increased in the spleen and tumors of the mGPRC5D-immunized mice compared with the respective percentages in the control group (Fig. 1G, H).

Evaluation of the therapeutic efficacy of the mGPRC5D vaccine used together with PD1 Ab against 5TGM1 tumors

We evaluated the therapeutic efficacy of the mGPRC5D vaccine combined with the PD1 Ab treatment. Following tumor inoculation, the mice received two injections of 20 μg mGPRC5D vaccine or the control plasmid at 2-week intervals, along with intraperitoneal administration of anti-PD1 antibody (50 μg per animal on days 9, 12, 15, and 18; Fig. 2A). Whereas mice treated with either mGPRC5D or anti-PD1 Ab showed a moderate inhibitory effect, those treated with the combination of mGPRC5D vaccination and PD-1 blockade exhibited significant inhibition of tumor development (Fig. 2B, C, Supplementary Fig. S1A, B). Furthermore, a comparison of tumor weights in mice revealed significantly lower weights in the mGPRC5D plus PD1 Ab group than in the control group or in each monotherapy (Fig. 2D). We further assessed the ability of the vaccine to induce TNFα or IFNγ responses in mouse splenocytes using the ELISPOT assay. Compared with controls, splenocytes from mice treated with mGPRC5D or PD1 Ab exhibited a significant increase in the number of spots, with a further increase noted in the group treated with the combination (Fig. 2E). Additionally, analysis of Th1 cytokine secretion revealed higher frequencies of $TNFα^+CD8^+$, $IFNγ^+CD8^+$, $TNFα^+CD4^+$, and $IFNγ^+CD4^+$ T cells in the spleen of mice in the combination therapy compared with that in the spleen of mice the monotherapy or control groups (Fig. 2F).

Next, we performed a flow cytometric analysis of immune cell populations in the spleen (Fig. 3A) and tumors (Fig. 3B). For $CD3^+$ T cells in the spleen, treatment with mGPRC5D increased the frequency of $CD4^+$ T cells by more than 150% and that of $CD8^+$ T cells by more than 30%; PD1 Ab treatment increased the frequency of $CD8^+$ T cells and $CD4^+$ T cells by more than 100%. The combination had a more pronounced effect, with more than 350% increase in $CD4^+$ T cells and more than 130% increase in $CD8^+$ T cells. Similar results were observed for DCs, Mϕ, and NK cells in the spleen. For tumor-infiltrating lymphocytes (TILs), the mGPRC5D vaccine and PD1 Ab combination increased the population of $CD8^+$ and $CD4^+$ T cells, DCs, Mϕ, and NK cells more than did the monotherapies. The elevated levels of $CD4^+$ and $CD8^+$ T cells and $CD20^+$ B cells in the splenic red pulp regions and tumor tissues of mice treated with the mGPRC5D vaccine and anti-PD1 Ab were confirmed using immunohistochemical staining (Fig. 3C–F). Hematoxylin and eosin (H&E) staining revealed no gross or histological damage to the major organs of the treated animals, suggesting acceptable safety profiles for the DNA vaccine or its combination (Supplementary Fig. S1C).

Development of nanoplasmid-encoded human GPRC5D (hGPRC5D) vaccine

Because the peptide sequences of mGPR5D and hGPRC5D are only ~81% identical, a human version of the vaccine is required. We developed a nanoplasmid construct expressing human GPRC5D (Nano-hGPRC5D). Nanoplasmids exhibit higher target expression levels than gWIZ[28]. Concurrently, we constructed a lentiviral construct expressing hGPRC5D (pHOT-GPRC5D), along with the mCherry gene, using the pUltra-hot vector (Plasmid #24130 from Addgene). The exogenous expression of hGPRC5D in 293T and B16-F10 cells was confirmed (Fig. 4A). Next, we generated mouse colorectal cancer cell lines (MC38 and CT26) and a melanoma cell line (B16-F10) stably expressing hGPRC5D using a lentiviral system (Fig. 4B). The expression of hGPRC5D in these cells was validated using western blot analysis (Fig. 4C). Antigen expression in vivo was validated by measuring hGPRC5D expression in immunized mouse muscle tissues 5 days after IM injection of the Nano-hGPRC5D vaccine and EP (Fig. 4D). These findings confirmed the effective expression of the Nano-hGPRC5D vaccine in vitro and in vivo.

The prophylactic Nano-hGPRC5D vaccine suppresses hGPRC5D-positive tumors

We performed prophylactic studies to evaluate the efficacy of Nano-hGPRC5D against tumors expressing hGPRC5D. We immunized either C57BL/6 mice (for MC38 and B16-F10; $n = 5$/group) or BALB/c mice (for CT26 model; $n = 5$/group) following a schedule of prime-boost at 2-week intervals, with 20 μg of Nano-hGPRC5D or a control plasmid (Nano-EGFP), delivered IM followed by EP (Fig. 5A, Supplementary Figs. S2, S3 and S4). Seven days after the second immunization, each mouse received a SC injection of 3×10^5 hGPRC5D-expressing MC38, B16-F10, or CT26 cells

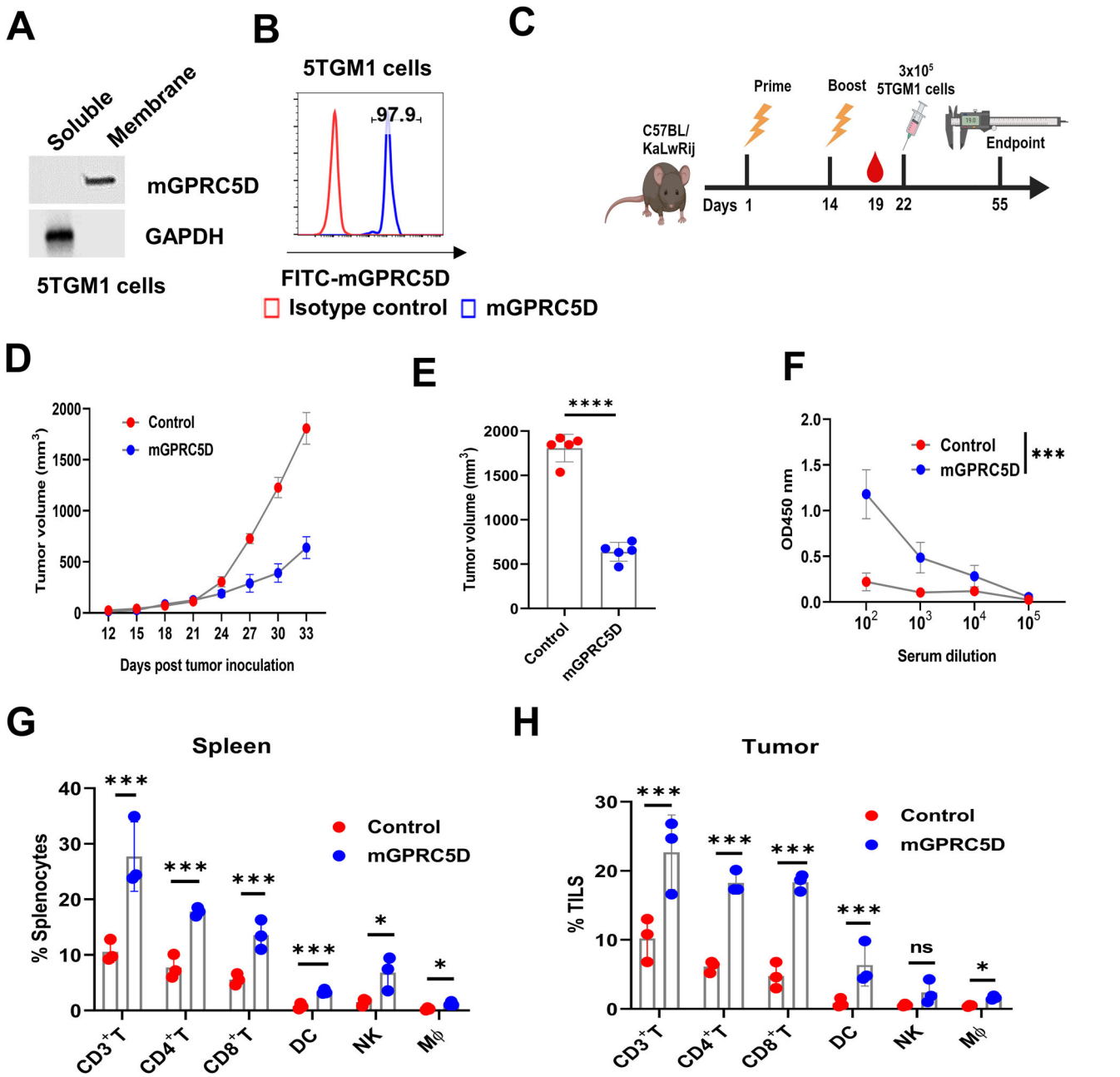

Fig. 1 | Prophylactic mGPRC5D vaccination inhibits tumor growth in the 5TGM1 murine model of MM. A Endogenous expression of mGPRC5D in the membrane fraction of 5TGM1 cells assessed using western blot analysis. **B** Quantification of mGPRC5D expression in 5TGM1 cells that were fixed but not permeabilized using flow cytometry. **C** Experimental workflow for prophylactic mGPRC5D vaccination (created using biorender.com). Mice were immunized twice at 14-day intervals by IM injection and EP. **D**, **E** Tumor volume measurements for assessing tumor growth, with the endpoint predefined by significant tumor burden. **F** Antibody titers 5 days post-second immunization, measured using ELISA; mGPRC5D recombinant protein (1 μg/mL) was used as the coating antigen. **G**, **H** Immune cell subsets, namely $CD3^+$, $CD4^+$, and $CD8^+$ T cells, DCs, NK cells, and Mϕ, in the spleen (**G**) and tumors (**H**), quantified using flow cytometry.

in the right flank. In each model, tumor growth in mice administered Nano-hGPRC5D was significantly suppressed compared with that in the control group (Fig. 5B, Supplementary Figs. S3B-D, Fig. S4B-D). We evaluated the humoral response in animals in the MC38 group to the Nano-hGPRC5D vaccine by collecting serum 5 days after the second vaccination and measuring the levels of the hGPRC5D-specific antibody with serum dilutions from 1:100 to 1:10,000. A marked increase in serum IgG levels was observed in the hGPRC5D vaccine group compared with that in the control mouse serum (Fig. 5C). Similarly, increased levels of hGPRC5D-specific serum IgG were observed in the hGPRC5D vaccine groups compared with those in the control groups in the B16-F10 and CT26 models (at 1:1000 dilution) (Supplementary Figs. S3E and S4E). We tested the ability of sera from immunized mice to detect membraneous hGPRC5D expression on MC38 cells using flow cytometry. The pooled sera from Nano-hGPRC5D-vaccinated mice bound to hGPRC5D on MC38 cells at a frequency of ~80% (Fig. 5D). Next, we measured the cytokine levels in sera collected 24 h after the boost from mice used in the MC38 model. A significant increase in the levels of cytokines (TNFα, IFNγ, IL-6, IL-12p40, and IL-12p70) was observed in the Nano-hGPRC5D vaccine group compared with the respective levels in the control group, indicating a robust activation of inflammatory cytokines upon Nano-hGPRC5D vaccination (Fig. 5E). To investigate the antitumor mechanisms of the Nano-hGPRC5D vaccine, we performed flow cytometry to analyze immune cells in the spleen and tumors from treated mice. The percentages of $CD3^+$, $CD4^+$, and $CD8^+$ T cells and

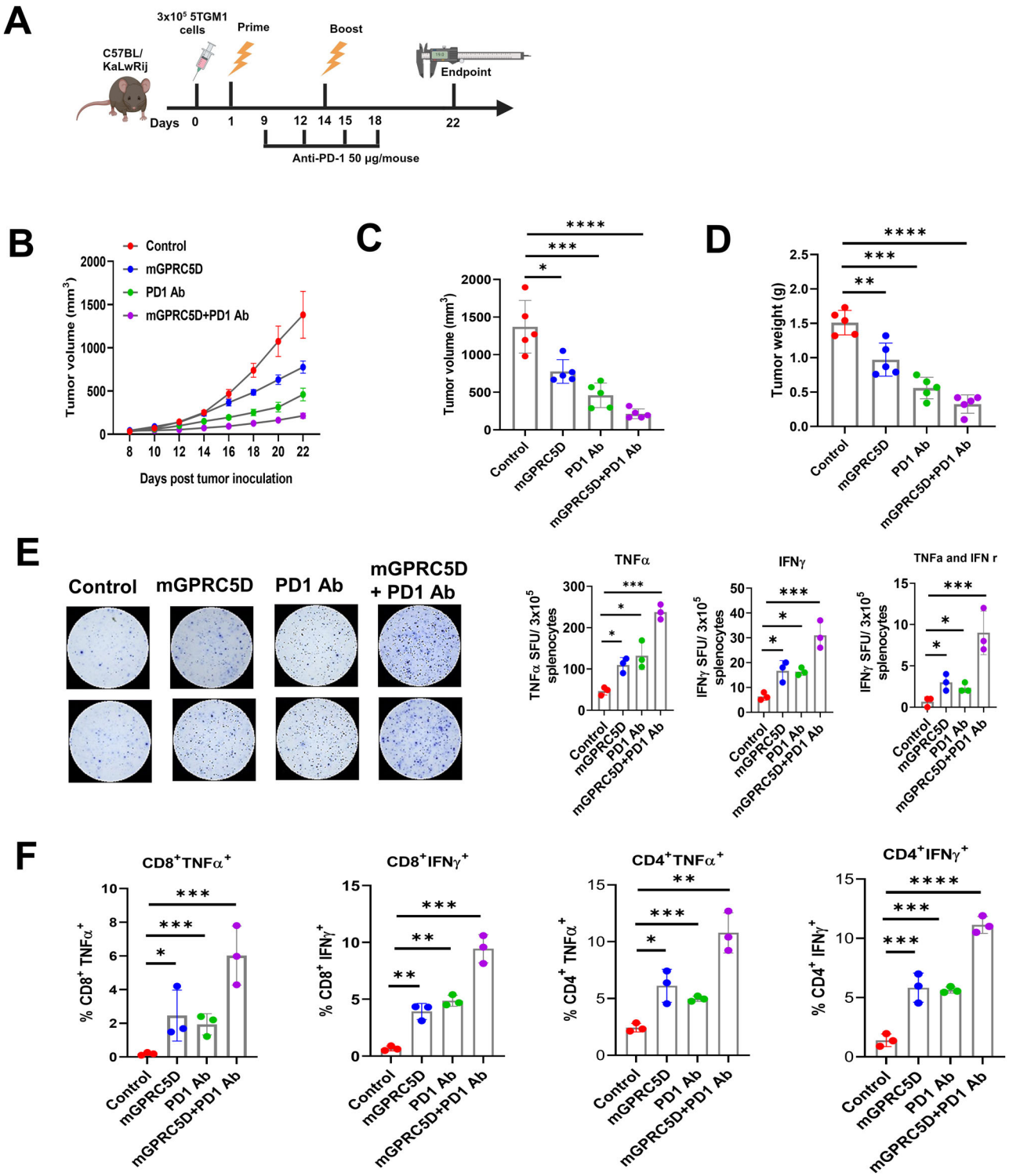

Fig. 2 | mGPRC5D vaccine and PD1 blockade suppress tumor growth in the 5TGM1 murine model of MM. A Experimental workflow for therapeutic mGPRC5D vaccination (created using biorender.com). **B**, **C** Tumor volume measurements. **D** Tumor weight at the endpoint. **E** Evaluation of antigen-specific TNFα- and IFNγ-secreting T cells using ELISpot assay. **F** Flow cytometric quantitation of $CD8^+TNF\alpha^+$, $CD8^+IFN\gamma^+$, $CD4^+TNF\alpha^+$, and $CD4^+IFN\gamma^+$ immune cells in the spleen of immunized mice.

DCs ($CD45^+CD11b^+CD11c^+$) were significantly increased in the spleen and tumors of hGPRC5D-immunized mice (Fig. 5F, G). Moreover, higher frequencies of Th1 secretory cytokine-positive $CD3^+$ T cells ($TNF\alpha^+CD4^+$, $IFN\gamma^+CD4^+$, $TNF\alpha^+CD8^+$, and $IFN\gamma^+CD8^+$ cells) were observed in the spleen and tumors of the hGPRC5D group (Fig. 5H, I). We next analyzed the expression of CD44 and CD62L, two memory T-cell markers, and found significantly higher percentages of effector ($CD44^{high}CD62L^{low}$) and central memory ($CD44^{high}CD62L^{high}$) T cells in the splenocytes in the hGPRC5D group (Fig. 5J, K), indicating a long-acting protective effect against tumors in the hGPRC5D group. As an efficacious antitumor response involves generating cytotoxic responses against the gene of interest, we assessed hGPRC5D-specific immune responses using T-cell proliferation, ELISpot,

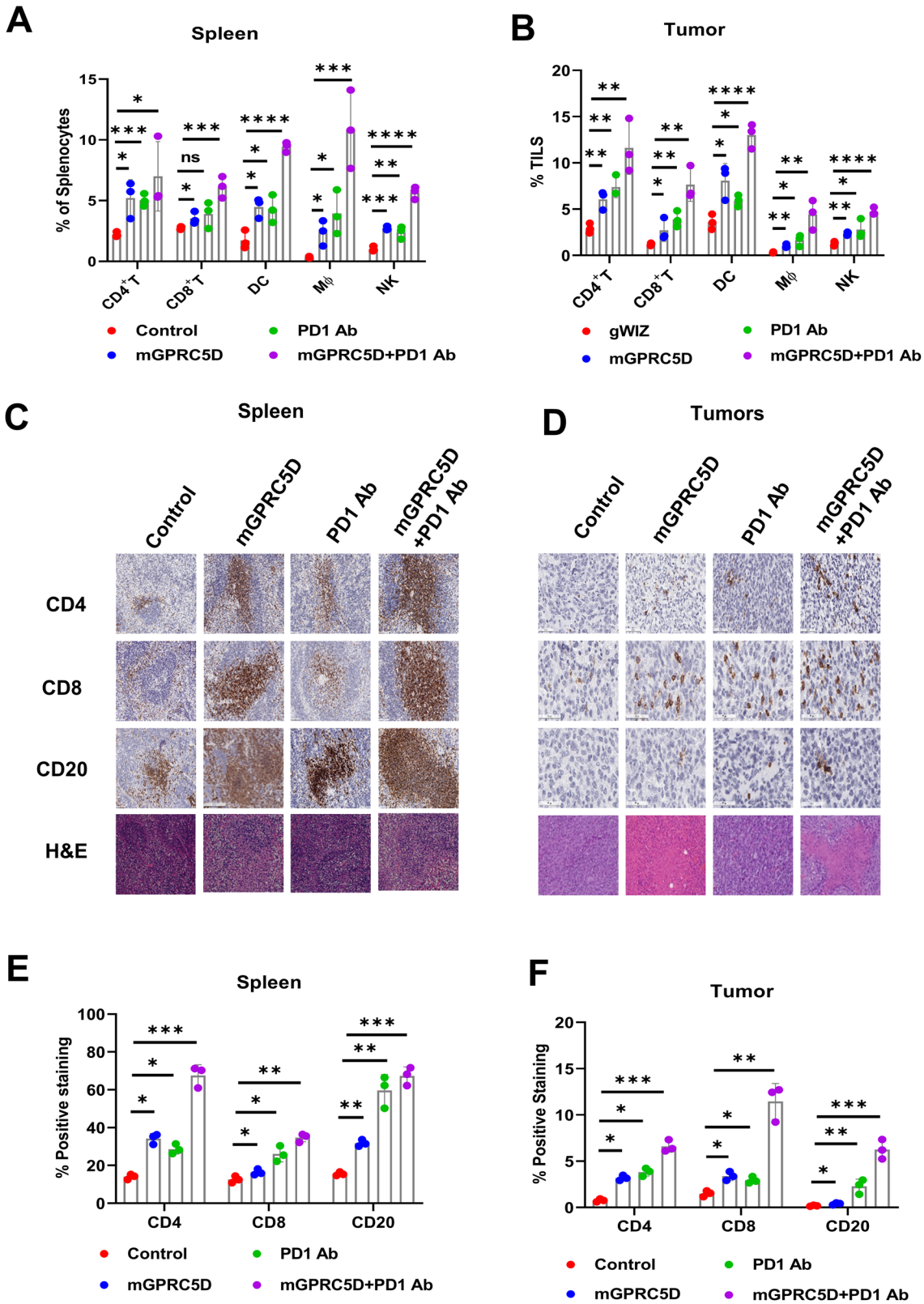

Fig. 3 | Flow cytometric and immunohistochemical analyses of the spleen and tumors from the 5TGM1 model. A, **B** Quantification of immune cell subsets in the spleen and tumors using flow cytometry. **C**, **D** Representative images (×20) of H&E and immunohistochemical staining of the spleen and tumor sections from the immunized mice (Scale bars = 50 μm). **E**, **F** Graphs representing the percentage of stained cells quantified using the ImageJ software.

and cytotoxic T lymphocyte (CTL) assays. $CD8^+$ T cells stimulated with the hGPRC5D peptide pool exhibited superior proliferative ability compared to the control, as confirmed using the EdU assay (Fig. 5L). Moreover, increased levels of TNFα- and IFNγ-secreting splenocytes were observed in the GPRC5D group (Fig. 5M). In addition, the effector $CD8^+$ T cells obtained from the splenocytes in the GPRC5D vaccine group almost completely cleared the MC38-hGPRC5D target cells, thus demonstrating potent cytotoxicity of antigen-specific $CD8^+$ T cells (Fig. 5N). These results

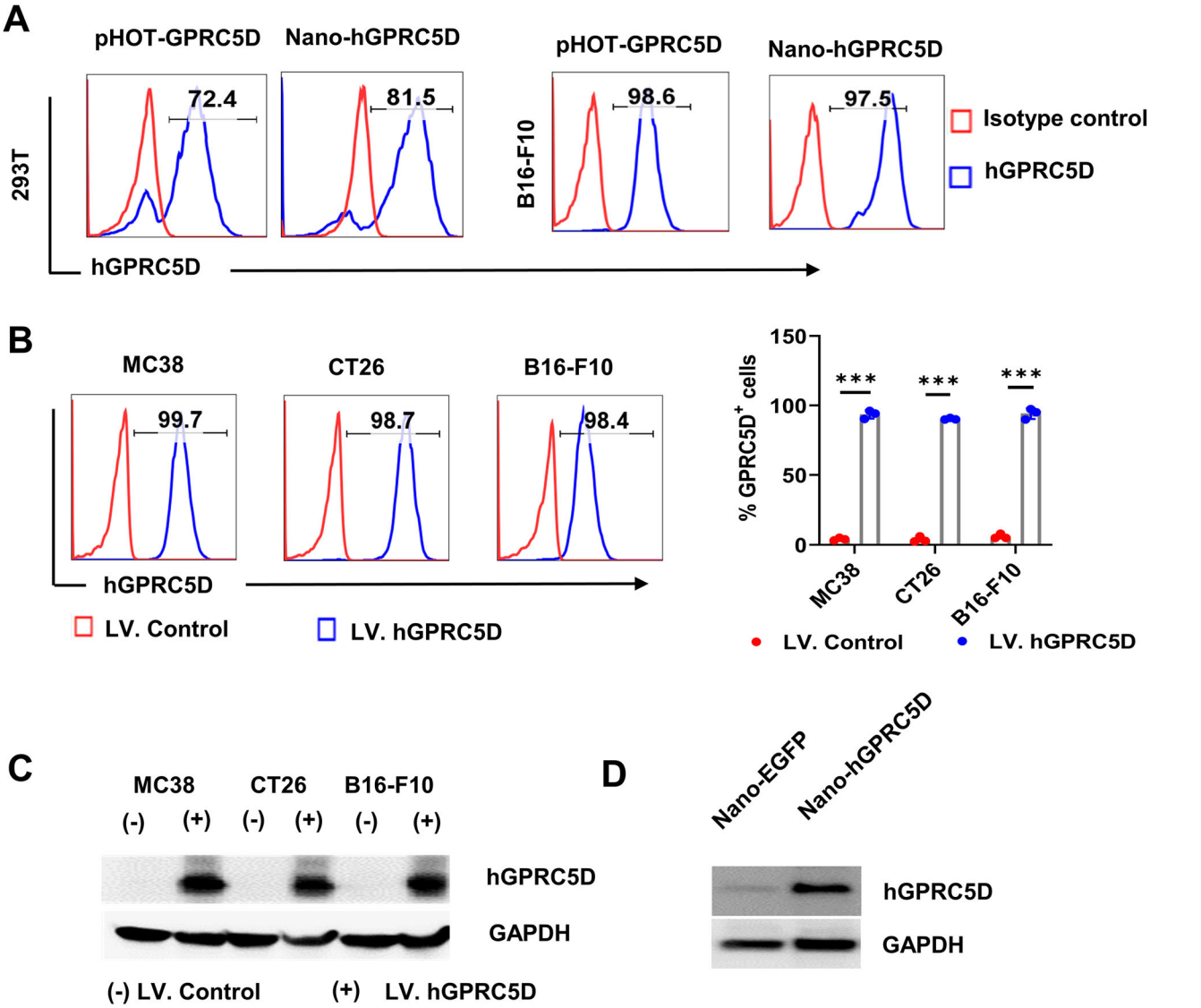

Fig. 4 | The recombinant nanoplasmid expressing hGPRC5D as a DNA vaccine candidate. A Flow cytometry analysis of exogenous hGPRC5D expressed in 293T or B16-F10 cells transfected with Nano-hGPRC5D or pUltraHot-hGPRC5D. **B**, **C** Flow cytometry and western blot analysis of hGPRC5D expression in mouse cells stably expressing hGPRC5D. **D** Western blot analysis of hGPRC5D expression in the muscle of C57/BL6J mice immunized with Nano-EGFP or Nano-hGPRC5D.

indicated that the GPRC5D vaccine triggered a potent CTL response against antigen-specific tumor cells.

Therapeutic efficacy of the nano-hGPRC5D vaccine used together with PD1 Ab in syngeneic mouse models

To evaluate the therapeutic efficacy of the Nano-hGPRC5D vaccine in combination with PD1 Ab treatment, we conducted experiments using syngeneic murine models. As for the prophylactic model, C57BL/6 mice were SC injected with MC38 or B16-F10 expressing hGPRC5D ($n = 5$/group), whereas BALB/c mice were injected with CT26 cells expressing hGPRC5D. Following tumor inoculation, mice were administered the Nano-hGPRC5D vaccine twice at 2-week intervals, along with either PD1 Ab (50 μg/mouse I.P.) or a control as outlined in Fig. 6A. The Nano-hGPRC5D vaccine showed moderate antitumor activity in all three models. However, the combination of the Nano-hGPRC5D vaccine and PD1 Ab resulted in significant tumor regression compared with that in either treatment alone (Fig. 6B, C, Supplementary Figs. S5A, B, S6A–D, S7A–D). In the CT26 model, two of the five tumors in the mice treated with the combination showed a complete response (Supplementary Fig. S7D). Weights of tumors from mice treated with the combination were significantly lower than those from the other groups (Fig. 6D, Supplementary Figs. S6E, S7E). The body weights of mice were similar (Fig. 6E, Supplementary Figs. S6F, S7F). Next, we measured cytokine production in the sera from treated mice in the MC38 model. The levels of TNFα, IFNγ, IL-6, IL-12p40, and IL-12p70 were significantly increased in sera from mice treated with the combination compared with the respective levels in the other groups (Fig. 6F). Additionally, ELISpot analysis of mouse splenocytes from vaccinated mice revealed more TNFα- or IFNγ-positive cells in the combination group than in the other groups (Fig. 6G). We performed a flow cytometric analysis of immune cell populations in the spleen and tumors. The Nano-hGPRC5D and PD1 Ab combination caused an increase in effector $CD8^+$ and $CD4^+$ T cells, DCs, Mϕ, and NK cells, but a decrease in T_{reg} cells (Fig. 6H, I). H&E staining of tumor sections revealed necrotic lesions in both the hGPRC5D and combination groups. However, no gross histological damage was observed in several major organs of the treated animals, indicating the safety and clinical potential of the DNA vaccine or the combination (Supplementary Fig. S5C). These findings indicated that the Nano-hGPRC5D and PD1 Ab combination inhibited tumor development by promoting the infiltration of immune cells into the tumors.

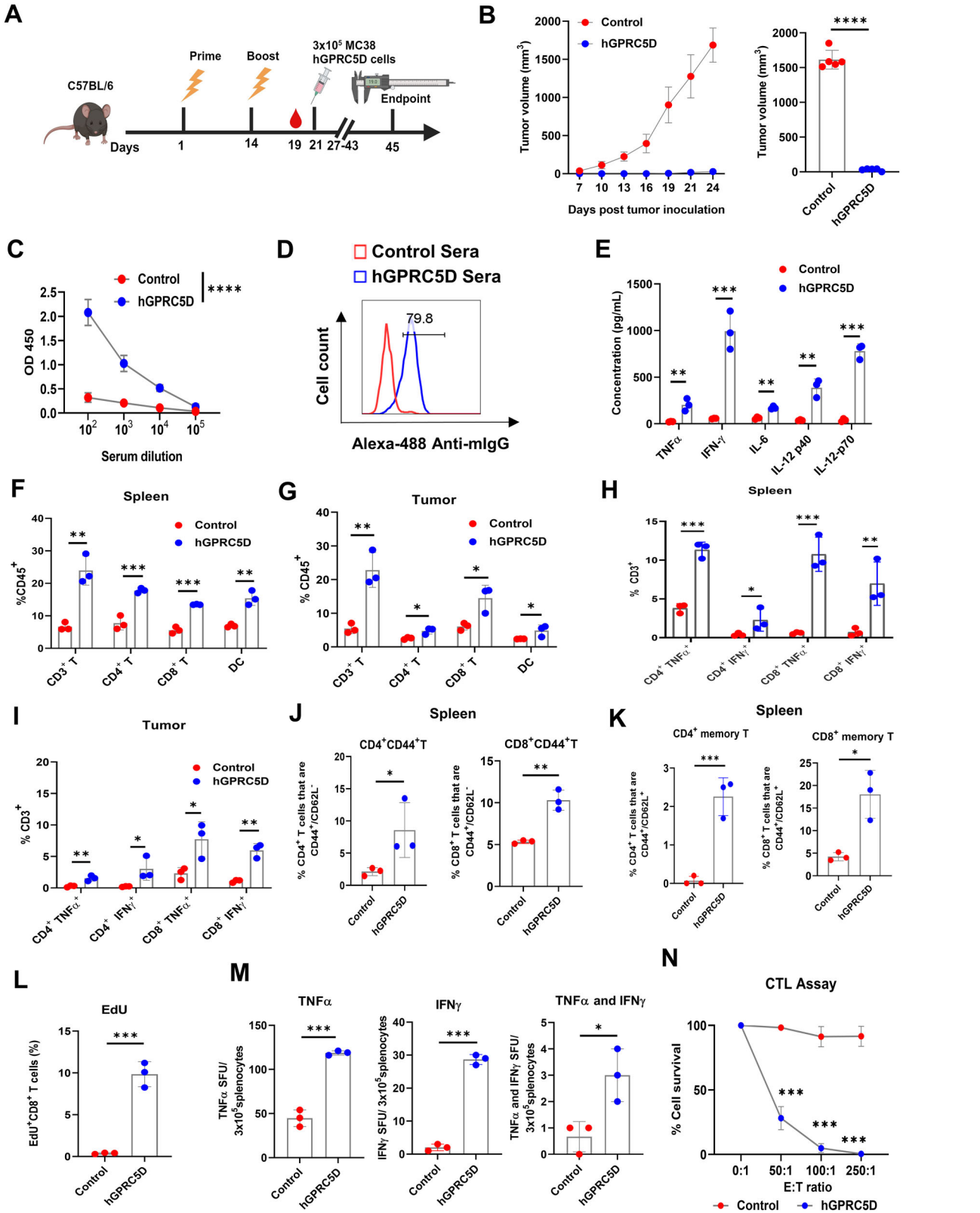

Fig. 5 | Nano-hGPRC5D inhibits tumor growth in a prophylactic model. **A** Experimental workflow for evaluating the prophylactic Nano-hGPRC5D vaccine (created using biorender.com). **B** Tumor volume measurements. **C** Antibody titers, 5 days after the second immunization, measured using ELISA; hGPRC5D recombinant protein (1 μg/mL) was used as a coating antigen. **D** Flow cytometric analysis of the binding of hyperimmune mouse sera to hGPRC5D expressed on the surface of MC38-hGPRC5D cells. Alexa-488 anti-mIgG was used as a secondary antibody. **E** Quantitation of serum cytokines using multiplex ELISA. **F**–**K** Flow cytometric analysis of immune cell subsets from the spleen (**F**, **H**, and **J**) and tumors (**G**, **I**, and **K**) of immunized mice. **L** Proliferation ability of $CD8^+$ T cells was assessed using the EdU assay. **M** Evaluation of antigen-specific splenocytes using ELISpot assay. **N** CTL assay showing tumor cell apoptosis induced by effector T cells pulsed with the hGPRC5D peptide pool.

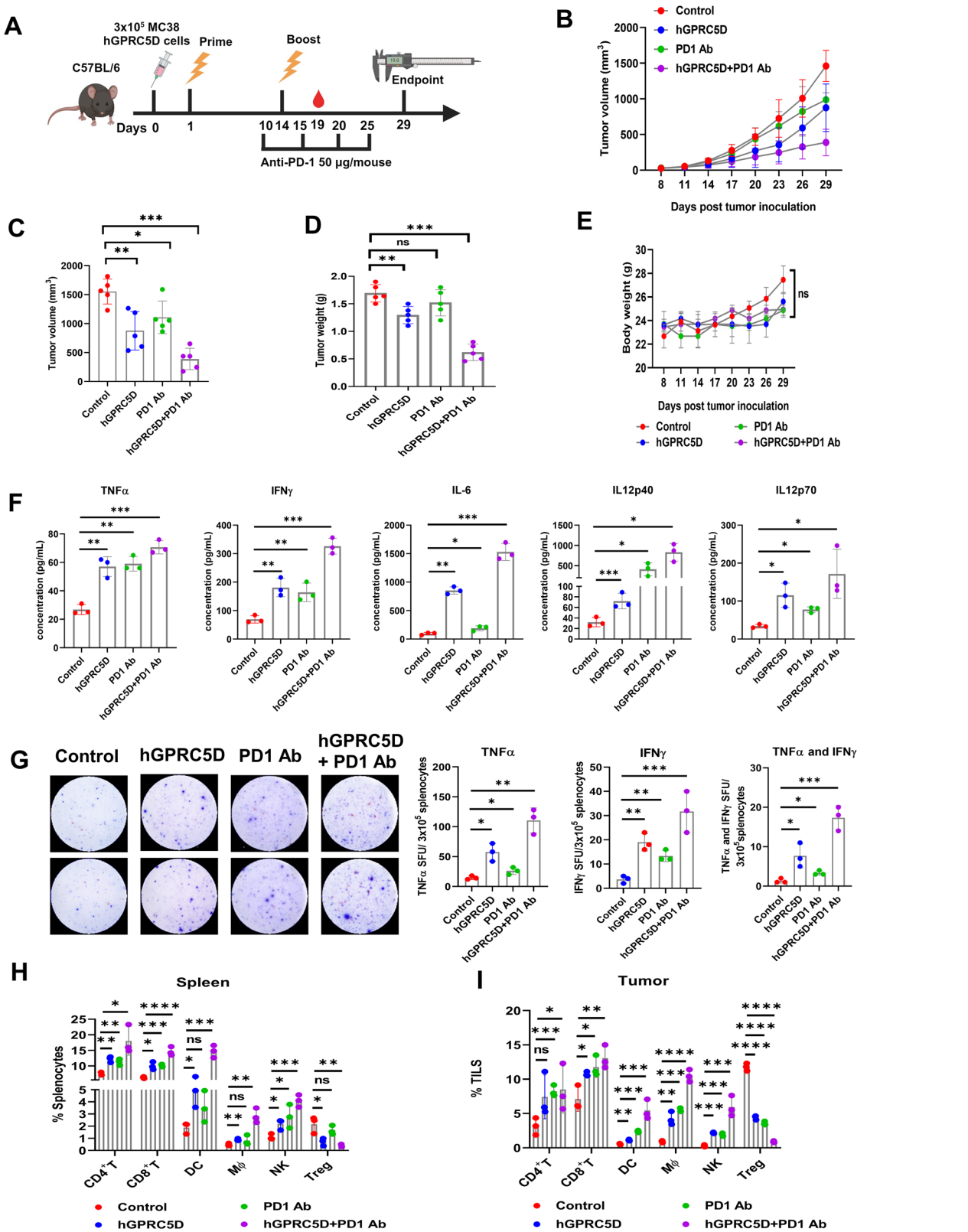

Fig. 6 | Nano-hGPRC5D, in combination with anti-PD-1 Ab, suppresses tumor growth in syngeneic mouse models. A Experimental workflow for evaluating the therapeutic Nano-hGPRC5D vaccine (created using biorender.com). The nano-hGPRC5D vaccine was tested alone and in combination with anti-PD1 Ab in C57/BL6J mice implanted with MC38 tumor cells expressing hGPRC5D. **B**, **C** Tumor volume measurements. **D** Tumor weight at the endpoint. **E** Changes in the body weight during treatment. **F** Plasma cytokine levels in vaccinated mice were determined using a Luminex multiplex ELISA assay. **G** TNFα and IFNγ double-color ELISpot assay of splenocytes from immunized mice stimulated with the hGPRC5D peptide pool. **H**, **I** Flow cytometric analysis of immune cell subsets in the spleen and tumors of immunized mice.

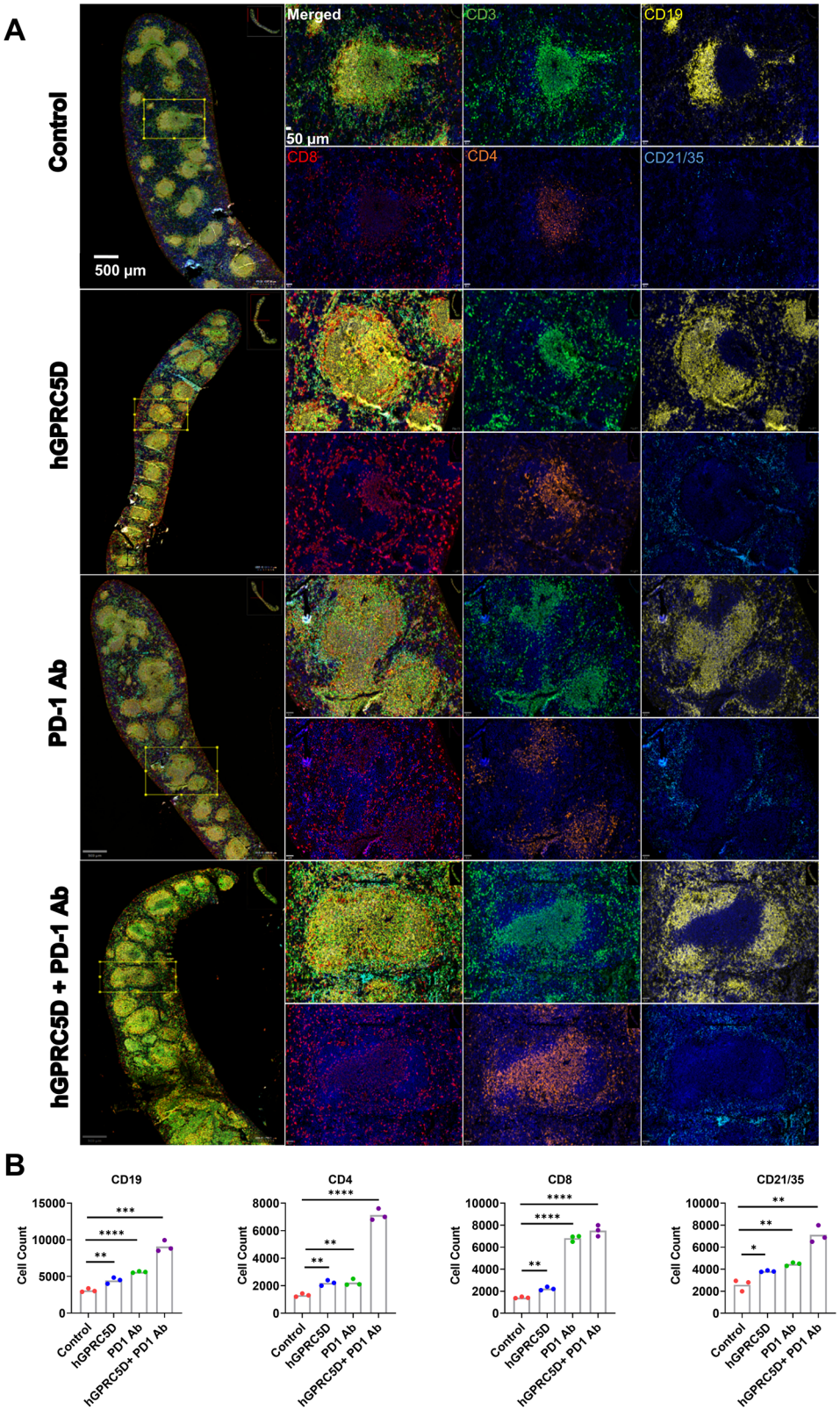

Fig. 7 | Evaluation of the altered immune cell populations in the spleen of immunized mice using mIF analysis. A Composite image of spleen sections (Scale bar = 500 μm) and germinal center (Scale bar = 50 μm) from immunized mice models followed by an image for each marker. Markers for CD3, CD19, CD8, CD4, and CD21/35 are in green, yellow, red, orange, and blue, respectively. The images were analyzed using the using the open-source software QUPATHv.4.4-m4. **B** Graphs illustrating the immune cell populations in the spleen sections.

Multiplex immunofluorescent (mIF) analysis of the immune cells in the spleen and tumors

Immune cells in the spleen and tumors of immunized mice were analyzed using the AKOYA PhenoCycler mIF platform. We used a custom mIF panel against five immune cell markers (CD3, CD4, CD8, CD19, and CD21/35) to stain the splenic sections (Fig. 7A). There was a marked increase in $CD3^+$, $CD8^+$ T, and $CD4^+$ T cells in the splenic marginal zones of the combination group compared with that in the monotherapy groups (Fig. 7A, B). These results were consistent with the flow cytometry data. We also observed an increase in B lymphocytes (CD19) and follicular DCs (CD21/35) in the spleen of mice in the combination group. For TILs, the combination therapy

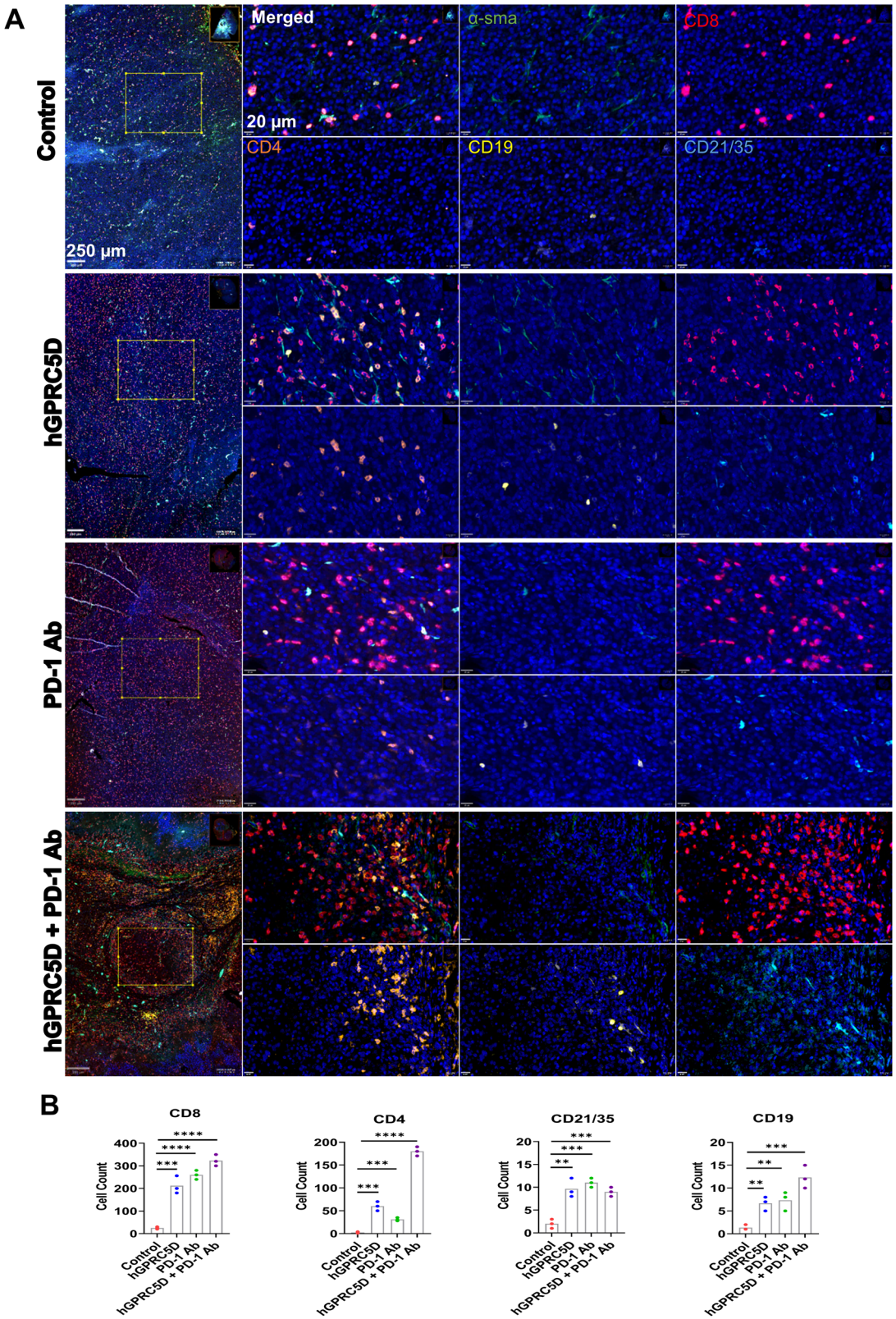

Fig. 8 | Evaluation of the altered immune cell populations in tumors of immunized mice using mIF analysis. A Representative images of tumor tissues depict markers for myofibroblasts (α-smooth muscle actin-green), CD8 (red), CD4 (orange), CD19 (yellow), and CD21/35 (Blue). **B** Graphs illustrating the immune cell populations in the tumor sections.

increased the number of $CD8^+$ and $CD4^+$ T cells (Fig. 8A), corroborating the flow cytometric data. We stained the tumor sections using five markers (α-smooth muscle actin [α-SMA], CD4, CD8, CD19, and CD21/35). The vaccination decreased the α-SMA levels and increased the levels of $CD8^+$ T and $CD4^+$ T cells, B cells, and follicular DCs (Fig. 8A, B). These data allow direct visualization of TILs and provide additional evidence to support the antitumor immunity elicited by the Nano-hGPRC5D vaccine and/or PD-1 Ab.

Discussion

MM is a genetically complex heterogeneous malignancy associated with substantial morbidity and mortality[29]. It accounts for 15–20% of all hematologic malignancies and has a 5-year survival rate of approximately 60%[1]. Although MM cells express various surface markers, such as CD38, CD138 (syndecan-1), and BCMA, GPRC5D has emerged as a notable target owing to its relatively exclusive expression on malignant plasma cells[30,31]. Moreover, its expression pattern is independent of BCMA, making it an attractive target, especially in patients who are resistant to or relapse after anti-BCMA therapies[32]. GPRC5D-targeting CAR-T therapies, antibody-drug conjugates (ADC), and bispecific antibodies (BsAb) have been developed. Recent phase II clinical trials of GPRC5D-targeted CAR-T, MCARH109, have shown an overall response rate of 58%[33]. LM-305, a GPRC5D ADC developed by Lanova Medicines, showed promising efficacy in early-phase trials[34]. Two BsAbs (teclistamab and talquetamab) targeting BCMA or GPRC5D and CD3 showed good clinical anti-MM activity and have been approved by the FDA to treat relapsed or refractory MM[35,36]. Despite advancements in therapies, high-risk patients with MM continue to have poor outcomes, and few agents have been developed to prevent MM or MGUS and SMM from progressing to MM. Therefore, we aimed to develop DNA vaccines that target MM surface antigens. DNA vaccines can be easily manufactured and distributed quickly, potentially reducing costs and increasing accessibility for patients with MGUS, SMM, and MM.

We used a nanoplasmid expressing full-length hGPRC5D as a vaccine candidate (Nano-hGPRC5D) against MM in a syngeneic mouse model. The Nanoplasmid vector (NTC9385R-eRNA41H-CpG RNA) has two adjuvant elements: (1) eRNA41H, which is a 114 bp RNA fragment that induces type-1 IFN production via the activation of retinoic acid-inducible gene 1 (RIG-1)[37] and (2) CpG RNA, which is a potential agonist of toll-like receptor 9 signaling that further activates DCs, Mϕ, and NK cells, leading to antigen presentation and production of cytokines[38,39]. DNA vaccines delivered via EP significantly increase the uptake of plasmid DNA in muscles by transiently permeabilizing cell membranes through electric impulses. This method results in a ~1000-fold increase in antigen delivery compared to that achieved with naked DNA injection[40]. EP also functions as an adjuvant by inducing inflammation and cytokine release and recruiting APCs, such as DCs and Mϕ[41,42]. Prophylactic vaccination with Nano-hGPRC5D and EP protected mice against tumorigenesis in several tumor cells expressing hGPRC5D by inducing memory effector and central memory $CD4^+$ and $CD8^+$ T cells. When Nano-hGPRC5D was combined with PD1 Ab to treat mice inoculated with hGPRC5D-positive tumor cells, robust antitumor humoral and cellular immune responses were elicited. In the CT26 model, complete tumor elimination was observed in two of five mice. However, tumors grew larger with either monotherapy, and no animals completely rejected the tumors in the CT26 or other models despite marked T-cell responses against hGPRC5D-expressing tumor cells. These results indicate that PD1 blockade enhances tumor growth inhibition in mice treated with the DNA vaccine. Despite numerous clinical trials of DNA vaccines against various cancers, none have targeted GPRC5D, making this study the first to validate the efficacy of anti-GPRC5D DNA vaccines against MM in mice.

Exogenous hGPRC5D expression in mouse cells eliminated the effect of self-tolerance. We used 5TGM1 cells derived from C57BL/KaLwRij mice to evaluate the mGPRC5D vaccine. Similar to Nano-hGPRC5D, the mGPRC5D DNA vaccine alone was potent in preventing 5TGM1 tumor growth in a prophylactic setting. However, PD1 blockade was required to inhibit the growth of established 5TGM1 tumors. This highlights the potential of the DNA-based GPRC5D vaccine to overcome self-tolerance and the prospects of advancing the Nano-hGPRC5D vaccine into clinical trials for patients with MM, SMM, or MGUS. In addition, we did not observe fur loss or other clinical signs of damage to the skin of mice treated with either mGPRC5D or hGPRC5D vaccines, in line with the data from anti-hGPRC5D CAR T cells in experimental animals[21].

Methods

Plasmid constructs

The hGPRC5D coding sequence was cloned into a 3rd generation lentiviral vector pUltra-hot (Addgene#24130) using BamHI and EcoRI downstream of mCherry-P2A to obtain bicistronic expression of mCherry and hGPRC5D. Subsequently, the recombinant plasmids were transformed into *Escherichia coli* DH5α competent cells and cultured overnight in Luria Bertani (LB) medium containing 100 mg/mL ampicillin. The Nano-hGPRC5D plasmid was generated by Nature Technology Corporation (now part of Aldevron) by subcloning hGPRC5D into NTC9385R-eRNA41H-CpG RNA using BamHI and EcoRI. For the gWIZ constructs, hGPRC5D and mGPRC5D coding sequences were cloned into the SalI and BamHI sites. All constructs were designed to express full-length hGPRC5D or mGPRC5D proteins (UniProt IDs: Q9NZD1 and Q9JIL6). All plasmids were validated using DNA sequencing. The plasmids were isolated and purified from bacteria using the Endo-Free Plasmid DNA Maxi Kit (ZymoPURE II, D4202, Zymo Research).

Animals and cell lines

Six- to eight-week-old C57BL/6 and BALB/c mice were purchased from the Jackson Laboratory (Bar Harbor, ME, USA) and maintained at the Baylor College of Medicine animal facilities. All procedures were performed according to protocols approved by the Institutional Animal Care and Use Committee (IACUC) at the Baylor College of Medicine. The human kidney cell line 293T and mouse cancer cell lines B16-F10, MC38, and CT26 were purchased from the American Type Culture Collection (Manassas, VA, USA). 293T, MC38, B16-F10, and CT26 cells were grown in complete DMEM or RPMI 1640 medium (ThermoFisher, Waltham, MA, USA) supplemented with 10% FBS and 1% penicillin/streptomycin in a humid environment containing CO_2 and air at 37 °C. 5TGM1 cells were a gift from Dr. Fenghuang Zhan (University of Arkansas for Medical Sciences, USA). All the cell lines were authenticated and regularly tested for mycoplasma contamination.

Western blot analysis

Cells were lysed in RIPA lysis buffer (ThermoFisher Scientific) containing a protease inhibitor cocktail and phosphatase inhibitors (ThermoFisher) and then collected and centrifuged at 12,000 rpm for 15 min at 4 °C. The supernatant was measured using the BCA protein assay reagent (ThermoFisher Scientific). The lysates were denatured in Laemmli sample buffer (Bio-Rad, Hercules, CA, USA) and resolved using Tris-glycine SDS-PAGE (4–20% polyacrylamide, Mini-PROTEAN Precast Gels, Bio-Rad). After transfer to a polyvinyl difluoride membrane, the membrane was blocked with 5% non-fat dry milk (Bio-Rad #1706404) in 0.1% TBS-Tween-20 for 2 h and incubated overnight with primary antibodies at 4 °C. Horseradish peroxidase (HRP)-conjugated anti-rabbit or anti-mouse IgG (Cell Signaling Technology [CST], Danvers, MA, USA) was used as a secondary antibody. Immunoreactive proteins were visualized using an enhanced chemiluminescence western blotting substrate (ThermoFisher Scientific; #34076). Antibodies against human GPRC5D (# PA5-102094) were obtained from ThermoFisher Scientific, anti-mouse GPRC5D from Abcam (ab55044), and anti-human GAPDH (CST Cat. #2118). Uncropped and unprocessed scans of all blots were provided in Supplementary Fig. S8.

Animal studies

C57BL/6J and BALB/c female mice (6 weeks old) were purchased from Jackson Laboratory. C57BL/KaLwRijHsd inbred mice were purchased from Envigo and maintained in the animal facility of Baylor College of Medicine under pathogen-free conditions. All procedures were performed with the approval of the IACUC of Baylor College of Medicine. Mouse immunization was performed as previously described[43]. Briefly, mice were anesthetized with an isoflurane induction chamber turned on at 2–3% with a flow

rate of 0.8–1.0 L/min. Then, 20 μg Nano-hGPRC5D plasmid or 20 μg empty vector in 20 μL nuclease-free water was injected into the anterior tibialis muscle of the shaved hind leg, followed by applying electrical fields with an amplitude of 250 V/cm pulses with a Trigrid electroporation (EP) device (ICHOR medical systems, San Diego, CA). Mice were administered a prime-boost immunization IM, followed by EP two weeks apart. Sera were collected for analysis on day 5 before and day 19 after the initial immunization. Tumor volumes were measured and calculated as (length × width × width)/2. When tumors reached the size criteria outlined by the ethics protocols, mice were euthanized by CO_2 inhalation method with a flow rate of 3 L/min, according to animal care protocols at Baylor College of Medicine.

Flow cytometry

The tumor tissues were excised and minced into approximately 1 mm^3 cubical pieces. They were digested using a mouse tumor dissociation kit (Miltenyi Biotec) and incubated on a rocker (Gentle MACS Octo 8; Miltenyi Biotec) at 37 °C for 30 min. The resulting digested cells were filtered through 70 μm cell strainers (BD Pharmingen) and washed twice with cold PBS containing 2% FBS. After blocking Fc receptors and removing dead cells with a Zombie Aqua Fixable Viability Kit (BioLegend), the cells were stained with anti-mouse CD45 (Biolegend #110730), CD3 (Biolegend #394145), CD4 (Biolegend #116008), CD8 (Biolegend #100734), CD62L (Biolegend #104430), CD44 (Biolegend #103030), CD11c (Biolegend #117335), CD11b (Invitrogen #46011282), F4/80 (Invitrogen #MF48017), NK1.1 (Biolegend #108735), IFN-γ (Biolegend #505810), and TNFα (Biolegend #506315) for 30 min at room temperature in the dark. Finally, the samples were analyzed using a Cytec NL-3000 flow cytometry system, and the data were analyzed using the FlowJo V10 software (BD 200 Biosciences).

Cytotoxic killing assay

$CD8^+$ T cells isolated from immunized mouse splenocytes were cultured in RPMI 1640 medium containing IL-2 (50 U/mL) and hGPRC5D peptide pool (5 μg/mL) for 5 days at 37 °C under a 5% CO_2 atmosphere. The primed cells were washed and suspended in the medium as effector cells. Thereafter, effector and target cells (MC38-hGPRC5D) were cocultured for 3 days in a 96-well plate at different ratios under a 5% CO_2 atmosphere at 37 °C. The cells were collected, stained with anti-mouse CD8α and anti-human GPRC5D, and analyzed using flow cytometry analysis. The specific killing rate of the CTL was calculated to determine the killing effect on tumor cells.

Detection of $CD8^+$ T-cell proliferation

$CD8^+$ T cells were isolated from single-cell suspensions prepared from immunized mouse splenocytes using a $CD8a^+$ T-cell isolation kit (Miltenyi #130104075) and were suspended in a culture medium containing IL-2 (50 U/mL) and 5 μg/mL of hGPRC5D peptide pool, seeded at a density of 3×10^5 cells/well in 96-well tissue culture plates and incubated for 72 h; the culture medium was refreshed, and the culture was continued for 48 h. Proliferation analysis was performed using the Click-iT EdU Alexa Fluor 647 Flow Cytometry Assay Kit (ThermoFisher Scientific; #C10424). In brief, lymphocytes were incubated with 10 μM EdU at 37 °C for 2 h, collected, and stained with Alexa Fluor 647-conjugated anti-CD8α for 30 min. The cells were then fixed, permeabilized, and rinsed before being exposed to 100 μL of the click reaction cocktail for 30 min. Finally, the cells were washed three times with the permeabilization buffer. Flow cytometry was performed to analyze the percentage of EdU^+ cells among $CD8^+$ T cells, and the proliferation rate was calculated.

Preparation of splenocytes

The spleens were aseptically removed and placed in an ice-cold RPMI/FBS medium. To generate a single-cell suspension, the tissue was placed in a 100 μm cell strainer mesh in a Petri dish containing 5 mL ice-cold RPMI/FBS and mashed with the plunger of a 3 mL syringe. The cell suspension was transferred into a 15 mL tube, and centrifuged at 300 × *g* for 5 min at 4 °C. The pellet, thus obtained, was resuspended in ACK (ammonium-chloride-potassium) lysis buffer. The lysis was stopped with 5 mL of ice-cold RPMI/FBS, and the lysate was centrifuged at 300 × *g* for 5 min. The splenocytes were cultured in RPMI containing 200 U/mL IL-2.

IgG ELISA

For binding and quantifying serum antibodies, ELISA 96-well plates (Corning#9018, USA) were coated overnight with 1 μg/mL of the human GPRC5D protein at 4 °C and blocked with 5% skim milk in PBS for 2 h at room temperature. Next, the plates were washed and incubated with diluted mouse sera (1:100–1:100000) for 2 h. Following incubation with primary serum, the plates were washed and incubated with HRP-conjugated anti-mouse IgG (CST; #7076) antibody for 1 h at room temperature. The plates were developed with 3, 3′, 5, 5′-tetramethylbenzidine (TMB; Sigma #T0440). The reactions were stopped with 1 N hydrochloric acid, and absorbance was measured at 450 nm using a microplate reader (*CLARIOstar*, BMG Labtech).

TNF-α and IFN-γ ELISpot assay

ELISpot assays were performed according to the manufacturer's instructions (CTL-Murine IFN-γ/TNF-α Double-Color Enzymatic ELISPOT Assay). Spleens from the immunized mice were harvested and stored in RPMI 1640 medium before dissociation using a stomacher. RBCs were removed using ACK lysis buffer. The splenocytes were then filtered and counted. The splenocytes (3×10^5/mL) were plated into each well and stimulated for 24 h with 15-mer peptides (overlapping by 11 amino acids) spanning the full-length protein sequence of the human or mouse GPRC5D (peptide 2.0) at a concentration of 5 μg/mL in the ELISpot plate (precoated with IFNγ and TNFα capture antibodies). As a negative control, cells were not stimulated with the peptides. The cells were washed off, and the plates were developed using biotinylated anti-TNFα and FITC anti-IFNγ detection antibodies, followed by treatment with a streptavidin-enzyme conjugate or FITC-HRP at 1:1000 dilution that resulted in visible spots. After the plates were developed, the spots were scanned and quantified using an Immunospot CTL reader (Shaker Heights, OH, USA). Blue spots represented the TNFα spots, and red spots represented the IFNγ spots. Spot-forming unit (SFU) per well was calculated, and the values are shown as the background-subtracted average of the measured samples.

Luminex assay

A multiplex mouse cytokine/chemokine magnetic bead panel assay kit (MCYTOMAG-70K, Millipore Sigma) was used to measure the concentrations of IL-6, TNFα, IFNγ, IL-12p40, and IL-12p70, according to the manufacturer's instructions. As previously described, this assay was performed by the Advanced Technology Cores at the Baylor College of Medicine. Briefly, 25 μL of the serum samples were added to a plate containing beads linked with antibodies and incubated overnight at 4 °C with shaking. The plate was then incubated with biotinylated detection antibody for 60 min at room temperature with shaking. After washing the plate, 25 μL of the detection antibody was added, and the plate was incubated for 60 min at room temperature and subsequently rewashed. Reading buffer was added to the wells, and each sample was measured in duplicate. The plates were read using a Luminex 200 instrument with a lower bound of 50 beads per sample per cytokine. A set of standard curves was used to determine the cytokine concentrations.

Immunohistochemistry

Immunohistochemistry was performed using a fully automated workflow (HistoWiz Inc., Brooklyn, NY, USA) following standard operating procedures. Samples were processed, embedded in a paraffin, and sectioned at 5 μm. Immunohistochemistry was performed using standard protocols on a Bond Rx autostainer (Leica Biosystems) with enzyme treatment (1:1000). The antibodies used were as follows: CD20 (CST #70168), CD4 (ab #183685), and CD8 (CST #98941). The BOND Polymer Refine anti-rabbit HRP Detection (Leica Biosystems) was used according to the manufacturer's protocol. The sections were counterstained with hematoxylin,

dehydrated, and coverslipped using a Tissue Tek-Prisma and Cover Slipper (Sakura). Whole slide scanning (×40) was performed using an Aperio AT2 (Leica Biosystems).

mIF assay

The mIF analysis of the spleen and tumors was performed by staining the spleen and tumor sections of immunized mice using the Opal 5-color fluorescence immunohistochemistry kit (Akoya Biosciences, Marlborough, MA, USA) according to the manufacturer's protocol. The following primary antibodies were used: aSMA (1A4, Sigma), Ki67 (SP6, Abcam), CD11c (D1V9Y, CST), F4/80 (D2S9R, CST), Ly6g (1A8, Bio Legend), CD19 (D4V4B, CST), CD4 (4SM95, Invitrogen), CD8 (D4W2Z, CST), CD21/35 (7E9, Bio Legend), and CD31 (D8V9E, CST), CD3 (SP7, Abcam). Formalin-fixed paraffin-embedded sections were deparaffinized by heating the slides at 65 °C for 1 h and then incubating them in xylene baths (2 × 5 min). Tissue sections were rehydrated using an ethanol gradient (50 dips × 2 times in 100%, 95%, and 70% ethanol) and placed in water. Antigen retrieval (AR) was performed using Tris-EDTA buffer (pH9) (Abcam, ab93684) or citrate buffer (pH6) (Sigma, C9999) with 10% glycerol for 20 min in a pressure cooker set on high pressure. The slides were then cooled to room temperature (~30 min) in AR buffer. The tissue sections were blocked in animal-free blocking buffer solution (CST, 15019) for 10 min at room temperature and incubated in primary antibody for 2 h at room temperature or overnight at 4 °C. The sections were washed in TBS containing 0.05% Tween-20 (TBST, 50 dips × 3 times) and incubated with secondary antibodies conjugated with HRP-polymers (Abcam, ab214882 and ab214880; Akoya Biosciences, ARH1001EA; Vector Laboratories, PK-6100) for 15 min at room temperature. Tyramide signal amplification was performed using opal fluorophores (Akoya Biosciences, FP1487001KT, FP1488001KT, FP1495001KT, FP1497001KT, FP1501001KT, and FP1498) for 10 min at room temperature. The slides were washed in TBST (3 × 50 dips), counterstained with DAPI (2 μg/mL) for 5 min at room temperature, and mounted using ProLong Glass Antifade Mountant (Invitrogen, P36980). Images were acquired using a PhenoImager Fusion (Akoya Biosciences).

Quantification and statistical analysis

All statistical analyses were performed using the GraphPad Prism 8 software (GraphPad Software, San Diego, CA, USA). For all bar graphs, data are presented as means ± SD from three experiments. Student's *t*-test was used to compare two groups (the treatment and the control), whereas one- or two-way analysis of variance was used to compare two or more groups with multiple time points. A probability value of $p \le 0.05$ was considered statistically significant ($^{*}p < 0.05$, $^{**}p < 0.01$, $^{***}p < 0.001$, $^{****}p < 0.0001$).

Data availability

The data generated in this study are available upon request from the corresponding author.

Received: 29 May 2024; Accepted: 19 September 2024;
Published online: 01 October 2024

References

1. Kumar, S. K. et al. Multiple myeloma. *Nat. Rev. Dis. Prim.* **3**, 17046 (2017).
2. Siegel, R. L., Miller, K. D., Wagle, N. S. & Jemal, A. Cancer statistics, 2023. *CA Cancer J. Clin.* **73**, 17–48 (2023).
3. Kyle, R. A. et al. Long-term follow-up of monoclonal gammopathy of undetermined significance. *N. Engl. J. Med.* **378**, 241–249 (2018).
4. Kyle, R. A. et al. Prevalence of monoclonal gammopathy of undetermined significance. *N. Engl. J. Med.* **354**, 1362–1369 (2006).
5. Kyle, R. A. et al. Clinical course and prognosis of smoldering (asymptomatic) multiple myeloma. *N. Engl. J. Med.* **356**, 2582–2590 (2007).
6. Kyle, R. A. et al. A long-term study of prognosis in monoclonal gammopathy of undetermined significance. *N. Engl. J. Med.* **346**, 564–569 (2002).
7. Davila, M. L. et al. Efficacy and toxicity management of 19-28z CAR T cell therapy in B cell acute lymphoblastic leukemia. *Sci. Transl. Med.* **6**, 224ra25 (2014).
8. Kantarjian, H. et al. Blinatumomab versus chemotherapy for advanced acute lymphoblastic leukemia. *N. Engl. J. Med.* **376**, 836–847 (2017).
9. Wang, X. et al. Expanding anti-CD38 immunotherapy for lymphoid malignancies. *J. Exp. Clin. Cancer Res.* **41**, 210 (2022).
10. Park, J. H. et al. Long-term follow-up of CD19 CAR therapy in acute lymphoblastic leukemia. *N. Engl. J. Med.* **378**, 449–459 (2018).
11. Ali, S. A. et al. T cells expressing an anti–B-cell maturation antigen chimeric antigen receptor cause remissions of multiple myeloma. *Blood* **128**, 1688–1700 (2016).
12. Brudno, J. N. et al. T cells genetically modified to express an anti-B-cell maturation antigen chimeric antigen receptor cause remissions of poor-prognosis relapsed multiple myeloma. *J. Clin. Oncol.* **36**, 2267–2280 (2018).
13. Laurent, S. A. et al. γ-Secretase directly sheds the survival receptor BCMA from plasma cells. *Nat. Commun.* **6**, 7333 (2015).
14. Brudno, J. N. et al. T cells genetically modified to express an anti–B-cell maturation antigen chimeric antigen receptor cause remissions of poor-prognosis relapsed multiple myeloma. *J. Clin. Oncol.* **36**, 2267–2280 (2018).
15. Cohen, A. D. et al. Safety and efficacy of B-cell maturation antigen (BCMA)-specific chimeric antigen receptor T cells (CART-BCMA) with cyclophosphamide conditioning for refractory multiple myeloma (MM). *Blood* **130**, 505 (2017).
16. Fry, T. J. et al. CD22-targeted CAR T cells induce remission in B-ALL that is naive or resistant to CD19-targeted CAR immunotherapy. *Nat. Med.* **24**, 20–28 (2018).
17. Gardner, R. et al. Acquisition of a CD19-negative myeloid phenotype allows immune escape of MLL-rearranged B-ALL from CD19 CAR-T-cell therapy. *Blood* **127**, 2406–2410 (2016).
18. Gilman, A. G. G proteins: transducers of receptor-generated signals. *Annu. Rev. Biochem.* **56**, 615–649 (1987).
19. Sriram, K. & Insel, P. A. G protein-coupled receptors as targets for approved drugs: how many targets and how many drugs? *Mol. Pharm.* **93**, 251–258 (2018).
20. Mullard, A. Setting GPCRs free. *Nat. Rev. Drug Discov.* **22**, 347–348 (2023).
21. Smith, E. L. et al. GPRC5D is a target for the immunotherapy of multiple myeloma with rationally designed CAR T cells. *Sci. Transl. Med.* **11**, eaau7746 (2019).
22. Pillarisetti, K. et al. A T-cell-redirecting bispecific G-protein-coupled receptor class 5 member D x CD3 antibody to treat multiple myeloma. *Blood* **135**, 1232–1243 (2020).
23. Verkleij, C. P. M. et al. Preclinical activity and determinants of response of the GPRC5DxCD3 bispecific antibody talquetamab in multiple myeloma. *Blood Adv.* **5**, 2196–2215 (2021).
24. Braunstein, M., Weltz, J. & Davies, F. A new decade: novel immunotherapies on the horizon for relapsed/refractory multiple myeloma. *Expert Rev. Hematol.* **14**, 377–389 (2021).
25. Moreau, P. & Touzeau, C. T-cell redirecting bispecific antibodies in multiple myeloma: a revolution? *Blood* **139**, 3681–3687 (2022).
26. Radl, J., De Glopper, E. D., Schuit, H. R. & Zurcher, C. Idiopathic paraproteinemia. II. Transplantation of the paraprotein-producing clone from old to young C57BL/KaLwRij mice. *J. Immunol.* **122**, 609–613 (1979).
27. Garrett, I. R., Dallas, S., Radl, J. & Mundy, G. R. A murine model of human myeloma bone disease. *Bone* **20**, 515–520 (1997).
28. Williams, J. A. & Paez, P. A. Improving cell and gene therapy safety and performance using next-generation nanoplasmid vectors. *Mol. Ther. Nucleic Acids* **32**, 494–503 (2023).
29. Cowan, A. J. et al. Global burden of multiple myeloma: a systematic analysis for the global burden of disease study 2016. *JAMA Oncol.* **4**, 1221–1227 (2018).

30. Atamaniuk, J. et al. Overexpression of G protein-coupled receptor 5D in the bone marrow is associated with poor prognosis in patients with multiple myeloma. *Eur. J. Clin. Invest.* **42**, 953–960 (2012).
31. Cohen, Y., Gutwein, O., Garach-Jehoshua, O., Bar-Haim, A. & Kornberg, A. GPRC5D is a promising marker for monitoring the tumor load and to target multiple myeloma cells. *Hematology* **18**, 348–351 (2013).
32. Kodama, T. et al. Anti-GPRC5D/CD3 bispecific T-cell–redirecting antibody for the treatment of multiple myeloma. *Mol. Cancer Ther.* **18**, 1555–1564 (2019).
33. Mailankody, S. et al. GPRC5D-targeted CAR T cells for myeloma. *N. Engl. J. Med.* **387**, 1196–1206 (2022).
34. Huang, W. et al. Abstract 6020: Preclinical activity of LM-305 targeting G-protein-coupled receptor class 5 member D (GPRC5D) antibody drug conjugate for the treatment of multiple myeloma. *Cancer Res.* **82**, 6020–6020 (2022).
35. Moreau, P. et al. Teclistamab in relapsed or refractory multiple myeloma. *N. Engl. J. Med.* **387**, 495–505 (2022).
36. Chari, A. et al. Talquetamab, a T-cell–redirecting GPRC5D bispecific antibody for multiple myeloma. *N. Engl. J. Med.* **387**, 2232–2244 (2022).
37. Luke, J. M. et al. Coexpressed RIG-I agonist enhances humoral immune response to influenza virus DNA vaccine. *J. Virol.* **85**, 1370–1383 (2011).
38. Sato, Y. et al. Immunostimulatory DNA sequences necessary for effective intradermal gene immunization. *Science* **273**, 352–354 (1996).
39. Klinman, D. M., Yamshchikov, G. & Ishigatsubo, Y. Contribution of CpG motifs to the immunogenicity of DNA vaccines. *J. Immunol.* **158**, 3635–3639 (1997).
40. Sardesai, N. Y. & Weiner, D. B. Electroporation delivery of DNA vaccines: prospects for success. *Curr. Opin. Immunol.* **23**, 421–429 (2011).
41. Liu, J., Kjeken, R., Mathiesen, I. & Barouch, D. H. Recruitment of antigen-presenting cells to the site of inoculation and augmentation of human immunodeficiency virus type 1 DNA vaccine immunogenicity by in vivo electroporation. *J. Virol.* **82**, 5643–5649 (2008).
42. Ahlén, G. et al. In vivo electroporation enhances the immunogenicity of hepatitis C virus nonstructural 3/4A DNA by increased local DNA uptake, protein expression, inflammation, and infiltration of CD3+ T cells. *J. Immunol.* **179**, 4741–4753 (2007).
43. Neeli, P. et al. Comparison of DNA vaccines with AS03 as an adjuvant and an mRNA vaccine against SARS-CoV-2. *iScience* **26**, 107120 (2023).

Acknowledgements

The authors thank Dana Rae Tardiel-Cyril, Drs. Xinfang Yu, Shan Zhou, and Xu Wang for their help with the animal experiments and technical support. We thank the Antibody-based Proteomics Core at Baylor College of Medicine for technical assistance in performing the Luminex experiments. The authors thank Dr. Bonam Srinivas Reddy for reviewing the first draft of the manuscript and providing comments. Y.L. is a CPRIT Scholar in Cancer Research supported by the Cancer Prevention and Research Institute of Texas (RR190043).

Author contributions

P.N. and Y.L.: Conceived and designed the project; P.N. and P.M.: Performed the experiments and analyzed the data; P.M., X.P.H., and K.S.C.: Performed and analyzed the mIF experiments; P.N., P.M., D.C., D.Z., and K.H.Y.: Contributed reagents, materials, and analysis tools, and wrote, reviewed, and edited the manuscript; Y.L. helped to finalize the manuscript. All authors read and approved the final manuscript.

Competing interests

The authors declare no competing interests.

Additional information

Supplementary information The online version contains supplementary material available at https://doi.org/10.1038/s41541-024-00979-w.

Correspondence and requests for materials should be addressed to Praveen Neeli or Yong Li.

Reprints and permissions information is available at http://www.nature.com/reprints

Publisher's note Springer Nature remains neutral with regard to jurisdictional claims in published maps and institutional affiliations.

Open Access This article is licensed under a Creative Commons Attribution-NonCommercial-NoDerivatives 4.0 International License, which permits any non-commercial use, sharing, distribution and reproduction in any medium or format, as long as you give appropriate credit to the original author(s) and the source, provide a link to the Creative Commons licence, and indicate if you modified the licensed material. You do not have permission under this licence to share adapted material derived from this article or parts of it. The images or other third party material in this article are included in the article's Creative Commons licence, unless indicated otherwise in a credit line to the material. If material is not included in the article's Creative Commons licence and your intended use is not permitted by statutory regulation or exceeds the permitted use, you will need to obtain permission directly from the copyright holder. To view a copy of this licence, visit http://creativecommons.org/licenses/by-nc-nd/4.0/.

© The Author(s) 2024